*Progress In Electromagnetics Research, PIER 8, 1–30, 1994*

# A NOVEL RESONANT CIRCULAR ARRAY: IMPROVED ANALYSIS

*G. Fikioris, R. W. P. King, and T. T. Wu*



## 1. Introduction

This paper describes the properties of large resonant circular arrays of lossless cylindrical dipoles. The dipoles are identical, parallel, equispaced and nonstaggered. Only one dipole in the array is driven. Figure 1 shows the top view of a circular array with $N = 90$ elements. Figure 2 shows a possible realization with elements over a ground plane. Here, "resonance" means narrow peaks in the self- and mutual conductances at a resonant frequency. The circular array is the simplest form of a general closed-loop array. Initial considerations regarding resonances in large closed-loop arrays are summarized by King in [1]; this paper also points out the important possible connection between resonance and superdirectivity in large noncircular closed-loop arrays.

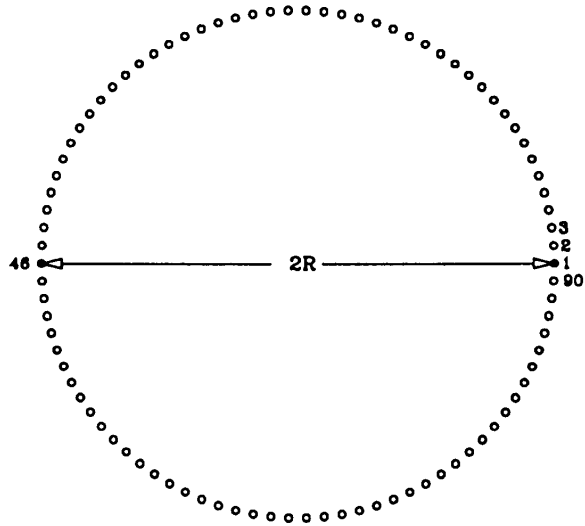


**Figure 1. Circular array with $N = 90$ elements.**

The idea that a large closed-loop array of cylindrical dipoles may possess narrow resonances originated from studies in quantum mechanics. It was found by Wu and Grossmann that an infinite linear array of Fermi pseudopotentials possesses resonances of zero width [2, 3], and that a large circular array of pseudopotentials possesses resonances the width of which is exponentially small in the number $N$ of pseudopotentials in the array [2]. Roughly speaking, a Fermi pseudopotential is a point interaction in the context of the Schrödinger equation, characterized by a single parameter with the dimension of length.

The case of a large closed-loop array of cylindrical dipoles is more involved. A dipole is characterized by its half-length $h$ and radius $a$. When used as a driven element in an antenna array, the currents in the dipole include components maintained directly by the generator as well as components induced by the currents in the other elements. If the dipole is parasitic, its current is due entirely to mutual coupling. The $N$ current distributions are the principal unknowns of the problem; they satisfy $N$ coupled integral equations which may be derived from Maxwell's equations. In the case of a circular antenna array, the

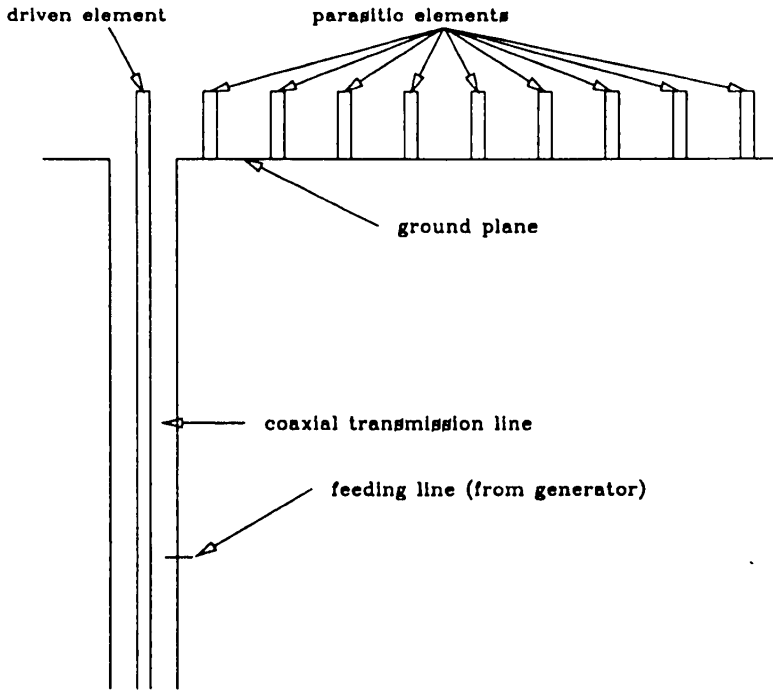


**Figure 2. Circular array of monopoles over ground plane. Driven element is extension of inner conductor of coaxial transmission line.**

equations may be decoupled via the "method of symmetrical components" [4]. Their solution is found by superimposing the solutions of $N$ independent integral equations.

The "two-term theory" of [4] is an approximate solution of the integral equations in which the current on a driven element in the array is represented as a linear combination of the two terms $\sin k(h - |z|)$ and $\cos kz - \cos kh$. The current on a parasitic element is of the form $\cos kz - \cos kh$. For the case of a circular array, there are closed-form expressions for the coefficients of the two components of current.

Despite the complexity of arrays of cylindrical dipoles, theoretical and experimental studies conducted in the past also supported the idea of the existence of narrow resonances in large closed-loop arrays [1]. For instance, it was known that the long Yagi array does not radiate broadside [5] and it was observed experimentally that this property is preserved if the array is bent into a semi-circle of sufficiently large radius [6].

Recently, theoretical studies have verified the existence of very narrow resonances in large circular arrays of cylindrical dipoles. In [7], resonances are illustrated graphically for 60-element and 90-element arrays. The currents are obtained using the original theory [4]. If $\lambda$ is the free-space wavelength, the values of the individual-element parameters are $h/\lambda = 0.18$ and $a/\lambda = 0.028$. The varying parameter is $d/\lambda$, where $d$ is the spacing between adjacent elements. Its value is very close to $0.3$ in the regions in which the narrow resonances occur. Also shown in [7] for each resonance is the radiation-field pattern in the horizontal plane. In this plane, the field has a flower-like shape where the nulls and maxima alternate rapidly.

In a subsequent paper, Freeman and Wu [8] re-examined the kernels used in the integral equations and derived a new set of kernels. With these kernels, the mutual interaction between elements is taken into account much more accurately than with the original kernels of [4]. As opposed to the original kernels of [4], the new kernels suggest the existence of *exponentially* narrow resonances in circular dipole arrays. However, use of these kernels in the two-term formulas presents difficulties because they are not of a simple form. A simpler alternative has been developed: the "modified" kernels (introduced in [9, 10] and here in Appendix A) possess the crucial properties of those developed in [8] while being even simpler in form than the original ones of [4]; they are obtained by setting $a = 0$ in the imaginary part of the original self-interaction kernel used in [4].

This paper makes use of the two-term theory of [4] but now applied with the modified kernel to develop conditions necessary for the existence of narrow resonances in circular arrays and to derive the properties of the resonant array. Section 2 contains the two-term theory in a new form convenient for the analysis of the circular array and lists the properties of the modified kernel. The two-term-theory formulas simplify considerably when the array is at resonance. These simplified formulas and the properties of the modified kernel are used

in Section 3 to derive the properties of the admittances (normalized midpoint currents) around the array when it is resonant. All currents are shown to be very large and to vary around the array with patterns characteristic of the particular resonance. Section 3 also illustrates how to choose the individual parameters $a/\lambda$ and $h/\lambda$, as well as the spacing $d/\lambda$ and the number of elements $N$ in order to excite a desired resonance. Section 4 examines the behavior of the admittances *near* a narrow resonance. Here, $d/\lambda$ is the variable but the conclusions are valid when the frequency is the variable and the geometrical parameters are fixed. An important conclusion is that the driving-point reactance always becomes zero near a narrow resonance. The patterns derived in Sections 3 and 4 for the current distributions around the array at or near a narrow resonance are applied in Section 5 to examine the radiation field in both the horizontal and the vertical planes. Simple approximate formulas are derived which show that the resonant array is highly directive in the vertical plane with field patterns that involve many sharp, pencil-like beams. Finally, Section 6 presents two refinements of the two-term theory that should be used when high accuracy is needed in actual numerical calculations. Theoretical results are then compared to experimental results.

If a resonant circular array is mechanically rotated about its axis, a fixed receiver close to the plane $\theta = \pi/2$ will see a series of pulses. The number of received pulses per minute is proportional to the angular speed of mechanical rotation. Thus, a rotating resonant circular array emits short pulses at a fixed rate and hence may be used as a microwave beacon which is easily identified by a receiver. Since microwave penetrates fog, such a beacon could have important advantages over optical beacons.

The subject of study in this paper is the large resonant circular array of lossless cylindrical dipoles with one dipole driven. The analysis may be extended to more complicated types of closed-loop arrays, such as: i) arrays with more than one driven element, and ii) arrays with noncircular shapes.

i) It has recently been shown [9, 11] that it is possible to generate a pancake-shaped field pattern (omnidirectional in the azimuth and highly directive in the vertical plane) by driving a second element in the circular array. Furthermore, both driving-point reactances may be zero if the parameters are properly chosen. A pancake-shaped field pattern is desirable in applications such as broadcast, ship-to-ship and

ship-to-shore communication.

ii) It has been pointed out [1] that it may be possible to determine a particular shape of closed-loop array that, when resonant, produces a highly directive field. The elliptical and the egg-shaped array are two possibilities. The conditions for resonance for a noncircular array should be similar to those developed here for a circular array as long as the minimum radius of curvature is sufficiently large. The analysis of the latter array is much more complicated and must rely on a thorough understanding of the former.

## 2. The Two-Term Theory and the Modified Kernel

Assume that element 1 of the circular array is driven by a voltage $V_1$ and that the rest of the elements $l = 2, \ldots, N$ are parasitic. The half-lengths and radii of the dipoles are $h$ and $a$, respectively, and the distance between adjacent elements is $d$. The two-term solution [4] is valid under the conditions $ka \ll 1$, $a \ll h < \lambda/4$ and $d \gtrsim h$ where $\lambda = 2\pi/k$ is the free-space wavelength. The condition $d \gtrsim h$ is used instead of the original condition $d/\lambda \geq \frac{1}{8}$ in light of recent investigations [12]. In this paper, only the case $N$ even is treated. (The formulation for $N$ odd is similar.) It follows from the method of symmetrical components that the $N$ currents $I_l(z)$, $l = 1, 2, \ldots, N$, are a superposition of the $N/2 + 1$ phase-sequence currents $I_1^{(m)}(z)$, $m = 0, 1, \ldots, N/2$. The two-term formulas in a notation convenient for the present purposes are the following:

$$I_l(z) = \begin{cases} \dfrac{j2\pi V_1}{\zeta_0 \Psi_{dR} \cos kh} [\sin k(h - |z|) + T_1(\cos kz - \cos kh)]; & l = 1, \\ \dfrac{j2\pi V_1}{\zeta_0 \Psi_{dR} \cos kh} T_l(\cos kz - \cos kh); & l = 2, 3, \ldots, N, \end{cases} \tag{1}$$

where $\zeta_0 = 376.73\ \Omega$. The parameter $\Psi_{dR}$ is real and independent of $N$ and $d/\lambda$. It is defined in Appendix B. The coefficients $T_l$ are complex and depend on all the parameters of the problem. They are obtained by superimposing the phase-sequence coefficients $T^{(m)}$:

$$T_l = \frac{1}{N}\left\{T^{(0)} - (-1)^l T^{(N/2)} + 2 \sum_{m=1}^{N/2-1} T^{(m)} \cos\left[\frac{2\pi(l-1)m}{N}\right]\right\}, \tag{2}$$

where

$$T^{(m)} = \frac{P_R^{(m)} + jP_I^{(m)}}{D_R^{(m)} + jD_I^{(m)}} = \frac{P_{1R} + P_{\Sigma R}^{(m)} + jP_I^{(m)}}{D_{1R} + D_{\Sigma R}^{(m)} + jD_I^{(m)}}. \tag{3}$$

In (3), the parameters in the numerator and the denominator are all real. They are given in terms of the various parts of the $m^{\text{th}}$ phase-sequence kernel in Appendix B. The subscript $I$ means that the parameter depends only on the imaginary part $K_I^{(m)}(z)$ of the modified phase-sequence kernel. Hence, $P_I^{(m)}$ and $D_I^{(m)}$ are independent of the radius $a/\lambda$. The subscript $1R$ means that the parameter depends only on the self-term $K_{1R}(z)$ of the real part of the kernel and is therefore independent of $N$, $m$ and $d/\lambda$. The subscript $\Sigma R$ means that the quantity depends only on the mutual terms $K_{\Sigma R}^{(m)}(z)$ of the real part of the kernel and is therefore independent of $a/\lambda$. The relation between $T^{(m)}$ and the phase-sequence admittances $Y^{(m)} = G^{(m)} + jB^{(m)}$ is

$$Y^{(m)} = \frac{j2\pi}{\zeta_0 \Psi_{dR} \cos kh} [\sin kh + T^{(m)}(1 - \cos kh)], \tag{4}$$

and the self- and mutual conductances $G_{1,l}$ (susceptances $B_{1,l}$) are determined only by the phase-sequence conductances $G^{(m)}$ (susceptances $B^{(m)}$):

$$G_{1,l} + jB_{1,l} = \frac{1}{N}\left\{ Y^{(0)} - (-1)^l Y^{(N/2)} + 2 \sum_{m=1}^{N/2-1} Y^{(m)} \cos\left[\frac{2\pi(l-1)m}{N}\right]\right\}. \tag{5}$$

The modified kernel (B7)–(B9) has been evaluated asymptotically for large $N$ and $d/\lambda$ fixed with $d/\lambda < m/N \leq \frac{1}{2}$ (see [8], [10], and also Appendix A). $K_{\Sigma R}^{(m)}(z)$ is well approximated by the kernel of the infinite linear array [replace $b_l$ by $ld$ in (B8) and let $N \to \infty$ while keeping $m/N$ fixed]; it is therefore roughly independent of $N$ for large $N$ and fixed $m/N$. The imaginary part $K_I^{(m)}(z)$ must be approximated more carefully because the imaginary part of the kernel

of the infinite linear array is exactly zero. The asymptotic formula for $K_I^{(m)}(z)$ is

$$\frac{K_I^{(m)}(z)}{k} \sim -\frac{1}{4\pi^{1/2}} \frac{1}{N^{1/2}} \frac{1}{[(m/N)^2 - (d/\lambda)^2]^{3/4}} \times \exp[-2N(m/N)g(x_m)] + \{\text{same with } m \to N - m\} \tag{6}$$

where

$$x_m = \frac{d/\lambda}{m/N}; \quad g(x) = \cosh^{-1}\left(\frac{1}{x}\right) - (1 - x^2)^{1/2}, \quad 0 < x < 1. \tag{7}$$

The approximation is better when $z/\lambda$ is small and when $d/\lambda$ is not very close to $m/N$. These are the cases of interest. When $m \ll N/2$, only the first term needs to be kept; in the extreme case of $m = N/2$, the second term simply contributes a factor of 2. The following properties of $K_I^{(m)}(z)$ are noted when $d/\lambda < m/N$:

Property 2.1: $K_I^{(m)}(z)$ is approximately independent of $z$.

Property 2.2: $K_I^{(m)}(z)$ is exponentially small in $N$ for fixed $d/\lambda$ and $m/N$.

Property 2.3: $K_I^{(m)}(z)$ is a rapidly decreasing function of $d/\lambda$ when $N$ and $m/N$ are fixed.

With Property 2.1, it follows that when $h/\lambda$ is not too large,

$$D_I^{(m)} \sim -2(\sin kh - kh\cos kh)\frac{K_I^{(m)}(0)}{k}; \qquad d/\lambda < m/N, \tag{8}$$

$$P_I^{(m)} \sim 2(1 - \cos kh)\frac{K_I^{(m)}(0)}{k}; \qquad d/\lambda < m/N, \tag{9}$$

so that $D_I^{(m)}$ and $P_I^{(m)}$ vary slowly with $kh$ and also possess the Properties 2.2 and 2.3.

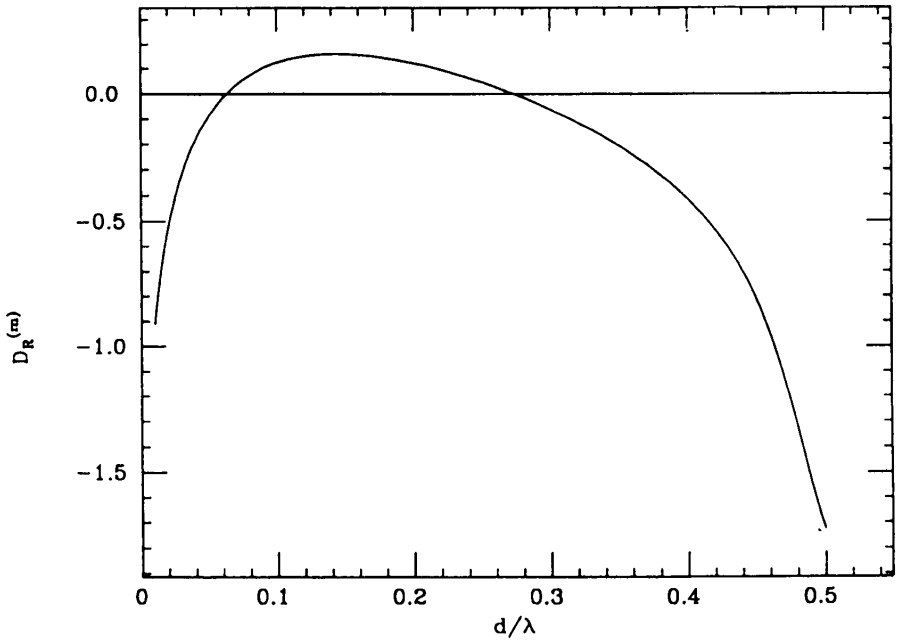


**Figure 3. Typical plot of $D_R^{(m)}$ as function of $d/\lambda$; $N = 90$, $m = 45$, $h/\lambda = 0.2$, and $a/\lambda = 0.05$.**

## 3. Phase-Sequence Resonances

Throughout this paper $d/\lambda$ is the variable and $a/\lambda$, $h/\lambda$, and $N$ are fixed, just as in the figures in [7]. In an actual application such as the experiments of [9] and [13], it is much simpler to vary the frequency and keep the geometrical parameters $a$, $h$, and $d$ fixed. The physical picture is very similar in the two cases.

A typical plot of $D_R^{(m)} = D_{1R} + D_{\Sigma R}^{(m)}$ as a function of $d/\lambda$ is given in Fig. 3. It is seen that $D_R^{(m)}$ is a quantity of order 1 that has two zeros in the range $0 < d/\lambda \leq 0.5$. The array is defined to be at its

$m^{\text{th}}$ phase-sequence resonance when $D_R^{(m)}$ is exactly zero. It will be seen that when this occurs, $G^{(m)}$ and $G_{1,1}$ are almost exactly at their maximum and $B_{1,1}$ is very close to its zero. In Fig. 3, the smaller root is not in the region of validity of the two-term theory since $d/\lambda < h/\lambda$. Since the position of the resonance is determined only by the real part of the kernel, a particular $m/N$ phase-sequence resonance will occur at roughly the same value of $d/\lambda$ for all large $N$. Here, it is assumed that the resonant spacing $d/\lambda$ is independent of $N$ so that it is meaningful to examine resonant currents as $N$ becomes larger while keeping $m/N$ and $d/\lambda$ fixed. Denote by $\delta_{m/N}$ the position of the larger root, so that $D_R^{(m)} = 0$ when $d/\lambda = \delta_{m/N}$. It is seen from (3) and (4) that, at the $m^{\text{th}}$ phase-sequence resonance,

$$T_{\text{res}}^{(m)} = \frac{P_I^{(m)}}{D_I^{(m)}} - j\,\frac{P_R^{(m)}}{D_I^{(m)}}, \tag{10}$$

$$G_{\text{res}}^{(m)} = \frac{2\pi}{\zeta_0 \Psi_{dR} \cos kh}\,\frac{P_R^{(m)}}{D_I^{(m)}}, \tag{11}$$

$$B_{\text{res}}^{(m)} = \frac{2\pi}{\zeta_0 \Psi_{dR} \cos kh}\left[\sin kh + (1 - \cos kh)\,\frac{P_I^{(m)}}{D_I^{(m)}}\right], \tag{12}$$

where $P_R^{(m)}$, $P_I^{(m)}$, and $D_I^{(m)}$ are evaluated at $d/\lambda = \delta_{m/N}$.

The quantity $P_R^{(m)}$ is of order 1. Because of Properties 2.2 and 2.3 and equations (8), (9), and (5), if $\delta_{m/N} < m/N$, it is seen that

Property 3.1: At the $m^{\text{th}}$ phase-sequence resonance, the phase-sequence conductance $G_{\text{res}}^{(m)}$ is extremely large in $N$. The self- and mutual conductances $G_{1,l}$ around the array are also extremely large and they vary around the array according to

$$G_{1,l} \propto G_{1,1} \cos\left[\frac{2\pi(l-1)m}{N}\right]; \quad l = 1, 2, \ldots, N. \tag{13}$$

This distribution of current around the array may be recognized as a standing wave.

Property 3.2: $G_{\text{res}}^{(m)}$ and the $G_{1,l}$'s will be much larger when the resonant spacing $d/\lambda = \delta_{m/N}$ occurs at a smaller value.

The conductances are actually predicted by (6), (8) and (11) to be *exponentially* large in $N$. This is a consequence of the assumption that the resonant spacing $d/\lambda = \delta_{m/N}$ does not depend on $N$ and may or may not be true within the two-term theory. Figure 4 shows the normalized conductances $G_{1,l}$ as a function of the element number $l$ for the $m/N = \frac{3}{8}$ phase-sequence resonance with $N = 72$. With $a/\lambda = 0.05$ and $h/\lambda = 0.2$, this occurs at $d/\lambda \simeq 0.2268$. The data in Fig. 4 as well as those of Figs. 5 and 6 and of Table 1 were obtained with the full two-term theory formulas (1)–(5) with the imaginary part of the kernel evaluated from (*B*9) using quadruple precision and with $T_{\text{res}}^{(m)}$ given by (10). In Fig. 4, the current distribution of Property 3.1 is recognized; in this case, the currents divide up into five groups. Note that $G_{1,1}$ is repeated at the end of Fig. 4 as $G_{1,73}$ for reasons of symmetry.

The parameter $D_R^{(m)} = D_{1R} + D_{\Sigma R}^{(m)}$ depends on $a/\lambda$ only through $D_{1R}$ and on $d/\lambda$ only through $D_{\Sigma R}^{(m)}$. By plotting $D_{1R}$ for various values of $h/\lambda$, it is seen that $D_{1R}$ is a decreasing function of $a/\lambda$, at least when $a/\lambda < 0.07$ and $a/\lambda \ll h/\lambda < 0.22$. (It can be shown, in fact, following a procedure similar to that in Appendix II of [14], that the variation with $a$ is linear in the quantity $\Omega = 2\ln(2h/a)$, but this approximation is poor when $h/a$ becomes small.) Hence, making the dipoles electrically thicker will result in decreasing the amplitude of a curve like that in Fig. 3, thereby shifting the resonant spacing $\delta_{m/N}$ to a smaller value of $d/\lambda$. The resonant currents will therefore become much larger. When the elements are electrically very thin, the array can have no narrow resonances at all, because the resonant root occurs at a value $d/\lambda > m/N$.

The effect of changing the length $h/\lambda$ is much more involved since both $D_{1R}$ and $D_{\Sigma R}^{(m)}$ depend on $h/\lambda$ in a complicated way. However, extensive numerical calculations show that the position of the root $\delta_{m/N}$ decreases when $h/\lambda$ increases, at least when $a/\lambda$ and $h/\lambda$ are in the above-mentioned ranges. Table 1 shows the resonant spacings $\delta_{m/N}$, the values of $K_I^{(m)}(0)$ evaluated at $d/\lambda = \delta_{m/N}$, and the self-conductance $G_{1,1}$ for 90-element arrays at their $m = N/2$

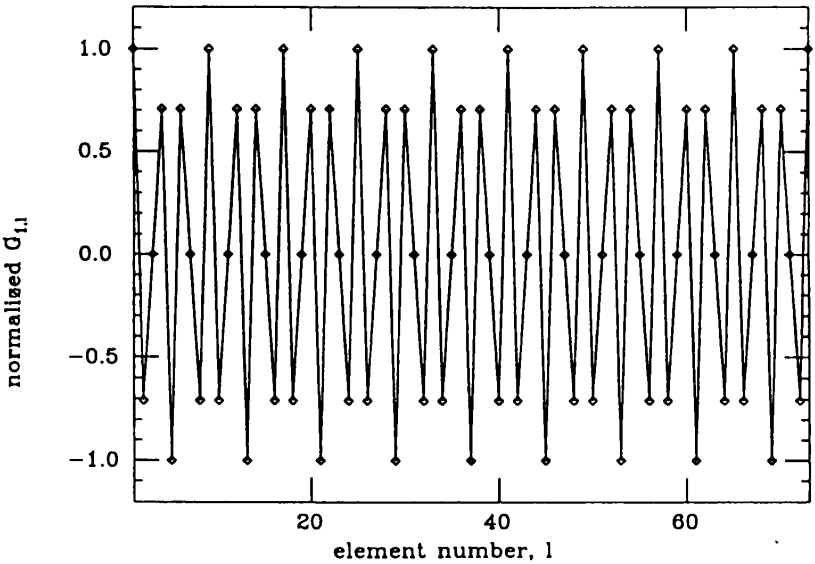


**Figure 4. Normalized self- and mutual conductances $G_{1,l}$ as function of element number $l$ for $m/N = \frac{3}{8}$ phase-sequence resonance; $N = 72$, $h/\lambda = 0.2$, $a/\lambda = 0.05$, and $d/\lambda = 0.22688$.**

phase-sequence resonance as $a/\lambda$ and $h/\lambda$ vary. The conclusion for $a/\lambda < 0.07$ and $a/\lambda \ll h/\lambda < 0.22$ is that

Property 3.3: If a specific phase-sequence resonance is desired, making the dipoles electrically longer or thicker will require an electrically smaller circle and will result in much higher resonant currents around the array.

| $h/\lambda$ | $a/\lambda = 0.01$ | $a/\lambda = 0.03$ | $a/\lambda = 0.05$ |
|---|---|---|---|
| 0.14 | no root | no root | $\delta_{m/N} = 0.479$<br>$\frac{K_I^{(m)}(0)}{k} = -0.25$<br>$G_{1,1} = 14.7$ mA/V |
| 0.16 | no root | $\delta_{m/N} = 0.480$<br>$\frac{K_I^{(m)}(0)}{k} = -0.18$<br>$G_{1,1} = 10.5$ mA/V | $\delta_{m/N} = 0.439$<br>$\frac{K_I^{(m)}(0)}{k} = -4.8 \times 10^{-3}$<br>$G_{1,1} = 81.6$ mA/V |
| 0.18 | $\delta_{m/N} = 0.494$<br>$\frac{K_I^{(m)}(0)}{k} = -0.47$<br>$G_{1,1} = 4.8$ mA/V | $\delta_{m/N} = 0.431$<br>$\frac{K_I^{(m)}(0)}{k} = -2.1 \times 10^{-3}$<br>$G_{1,1} = 109$ mA/V | $\delta_{m/N} = 0.370$<br>$\frac{K_I^{(m)}(0)}{k} = -3.9 \times 10^{-7}$<br>$G_{1,1} = 4.8 \times 10^5$ mA/V |
| 0.20 | $\delta_{m/N} = 0.437$<br>$\frac{K_I^{(m)}(0)}{k} = -4.1 \times 10^{-3}$<br>$G_{1,1} = 54$ mA/V | $\delta_{m/N} = 0.336$<br>$\frac{K_I^{(m)}(0)}{k} = -7.0 \times 10^{-10}$<br>$G_{1,1} = 2.1 \times 10^8$ mA/V | $\delta_{m/N} = 0.273$<br>$\frac{K_I^{(m)}(0)}{k} = -2.3 \times 10^{-16}$<br>$G_{1,1} = 6.3 \times 10^{14}$ mA/V |

**Table 1. Resonant spacings $d/\lambda = \delta_{m/N}$; values of the imaginary part of the kernel $K_I^{(m)}(0)/k$ at $z = 0$, $d/\lambda = \delta_{m/N}$; and the driving-point conductance $G_{1,1}$ at resonance. (Number of elements $N = 90$; phase sequence $m := N/2 = 45$. Roots $\delta_{m/N}$ are sought in the interval $h/\lambda < d/\lambda < \frac{1}{2} = m/N$.)**

It is seen from Table 1 that the currents are predicted to be extremely large when the perfectly conducting elements are long and thick. Very large currents can be realized in practice only with superconducting elements; in the case of *highly* conducting elements (for example, elements made from brass or aluminum), the currents are severely limited.

The superiority of the theory with the improved kernel $K_I^{(m)}(z)$ is illustrated here by two numerical examples: i) It is seen from Table 1 that the improved theory does not predict a very narrow resonance for the parameters $h/\lambda = 0.18$ and $a/\lambda = 0.028$ of [7]. With the original kernel $K_I^{(m)}(z)$, the value of $G_{1,1}$ at the $m = N/2$ resonance was predicted to be around 3,200 mA/V for these parameters. ii) If one attempts to apply the original theory for the parameters in the last entry of Table 1 ($h/\lambda = 0.2$ and $a/\lambda = 0.05$), a *negative* driving-point conductance ($G_{1,1} = -97$ mA/V) is obtained. Here, the original theory is obviously inadequate.

## 4. Behavior near a Phase-Sequence Resonance

Consider again that $a/\lambda$, $h/\lambda$, and $N$ are fixed, and that $d/\lambda$ is varied but stays very close to a resonant spacing $\delta_{m/N}$ so that the array is very close to its $m^{\text{th}}$ phase-sequence resonance. The function $D_R^{(m)}$ is usually a quantity of order 1, but near resonance it is of the order of magnitude of the very small quantity $D_I^{(m)}$; it is the controlling quantity in (3). It is a good approximation to assume that $P_R^{(m)}$, $P_I^{(m)}$, and $D_I^{(m)}$ are constant and that $D_R^{(m)}$ varies linearly with $d/\lambda$ so that the dependence of $T^{(m)}$ on $d/\lambda$ is explicitly

$$T^{(m)}(d/\lambda) = \frac{P_R^{(m)} + jP_I^{(m)}}{\alpha(d/\lambda - \delta_{m/N}) + jD_I^{(m)}}, \tag{14}$$

where $\alpha$ is the slope of $D_R^{(m)}$ near its zero. Using $P_R^{(m)} \gg P_I^{(m)}$, it is seen from (14) that $\mathrm{Re}\{T^{(m)}\}$ has extrema when $D_R^{(m)} \simeq \pm D_I^{(m)}$ or $d/\lambda - \delta_{m/N} \simeq \pm D_I^{(m)}/\alpha$ with

$$\mathrm{Re}\{T^{(m)}\} = \pm\frac{P_R^{(m)}}{2D_I^{(m)}} = \mp\frac{1}{2}\mathrm{Im}\{T_{\text{res}}^{(m)}\} = \mp\mathrm{Im}\{T^{(m)}\}. \tag{15}$$

From (4) and (5), it is seen that

Property 4.1: $B^{(m)}$ and the $B_{1,l}$'s are very rapidly varying near a narrow resonance. When the spacing $d/\lambda$ is such that $G^{(m)}$ has decreased to half its maximum value, $B^{(m)}$ is roughly equal to $G^{(m)}$: $B^{(m)} = \pm G^{(m)} = \pm\frac{1}{2}G^{(m)}_{\text{res}}$. Hence, $B^{(m)}$ and the $B_{1,l}$'s have a zero very close to resonance.

If, in (14), $P_I^{(m)}$ is neglected compared to $P_R^{(m)}$, a simpler formula for the behavior near a narrow resonance as a function of $d/\lambda$ (or as a function of frequency) is obtained which predicts a constant self-resistance and a linearly varying self-reactance which becomes zero at resonance.

## 5. Radiation Field at or near a Resonance

With the two-term theory currents, and with the center of the spherical coordinates $(r, \theta, \phi)$ placed at the center of the array, the radiation field is given by $\mathbf{E} = \widehat{\theta} E_\theta$, where [4]

$$E_\theta = -\frac{V_1}{\Psi_{dR}\cos kh}\frac{e^{-jkr}}{r}\left\{F(\theta)e^{jkR\sin\theta\cos(\phi-\phi_1)} + G(\theta)\sum_{l=1}^{N} T_l e^{jkR\sin\theta\cos(\phi-\phi_l)}\right\}. \tag{16}$$

In (16), $(R, \pi/2, \phi_l) = (R, \pi/2, 2\pi(l-1)/N)$ is the location of element $l$, $R = d/(2\sin\pi/N)$ is the radius of the circular array, and

$$F(\theta) = \frac{\cos(kh\cos\theta) - \cos kh}{\sin\theta}, \tag{17}$$

$$G(\theta) = \frac{\sin kh\cos(kh\cos\theta)\cos\theta - \cos kh\sin(kh\cos\theta)}{\sin\theta\cos\theta}. \tag{18}$$

The first term in (16) represents radiation from the sine current of the driven element; the second term is radiation from the shifted-cosine currents of all elements; $F(\theta)$ and $G(\theta)$ are the "element factors" for the sine and shifted-cosine currents, respectively. At or near a narrow resonance, we have the standing-wave distribution $T_l \simeq T_1 \cos[2\pi(l-1)m/N]$. It will be seen that the first term in (16) may be neglected. Thus, if one defines the array factor for the $m^{\text{th}}$ phase-sequence resonance as the radiation field due to an array of isotropic radiators with the $m^{\text{th}}$ phase-sequence currents around the array, with element 1 having unit current, viz.,

$$A^{(m)}(\theta,\phi) = \sum_{l=1}^{N} \cos\left[\frac{2\pi(l-1)m}{N}\right] e^{jkR\sin\theta\cos(\phi-\phi_l)}, \tag{19}$$

then the radiation field is given approximately by

$$E_\theta = -\frac{V_1}{\Psi_{dR}\cos kh}\frac{e^{-jkr}}{r} G(\theta) T_1 A^{(m)}(\theta,\phi). \tag{20}$$

The sum in (19) may be written exactly as follows (see [15] for a detailed derivation):

$$\begin{aligned} A^{(m)}(\theta,\phi) = {} & N \sum_{p=-\infty}^{\infty} j^{Np+m} J_{Np+m}[N(d/\lambda)\sin\theta] \\ & \times \cos[(Np+m)\phi]. \end{aligned} \tag{21}$$

Because of the condition $d/\lambda < m/N \leq \frac{1}{2}$, the arguments of the Bessel functions are always smaller than the orders. When $N$ is large, only two terms in (21) are significant, viz.,

$$\begin{aligned} A^{(m)}(\theta,\phi) \sim {} & N j^m J_m[N(d/\lambda)\sin\theta]\cos(m\phi) \\ & + \{\text{same with } m \to N-m\} \end{aligned} \tag{22}$$

As with the imaginary part of the kernel, the first term is adequate when $m \ll N/2$ and the second term is equal to the first one when

$m = N/2$. Assuming for simplicity that $m \ll N/2$ and using the asymptotic formula for the Bessel functions, one obtains

$$A^{(m)}(\theta,\phi) \sim j^m \frac{1}{(2\pi m/N)^{1/2}} \frac{1}{[1-(x_m \sin\theta)^2]^{1/4}} \times \exp[-N(m/N)g(x_m \sin\theta)] \cos(m\phi); \qquad m \ll N/2, \tag{23}$$

where $x_m$ and $g(x)$ are the same as in (7). Hence, the array factor is an exponentially small quantity and, in fact, it shares Properties 2.2 and 2.3 of $K_I^{(m)}(z)$. From (20), (23), and the expressions (8)–(10) for $T_1 \simeq (2/N)T_{\text{res}}^{(m)}$, it is seen that:

Property 5.1: The magnitude of the radiation field at any fixed point in space is extremely large in $N$.

This verifies that radiation from the sine current of element 1 is negligible and justifies the usefulness of the array factor. The largeness of the field should be expected since, for lossless elements, integration of $|E_\theta|^2$ over a large sphere should give the total radiated power $\frac{1}{2}G_{1,1}|V|^2$, which is large.

Property 5.2: The horizontal field pattern consists of $2m$ spikes.

Property 5.3: The vertical field pattern is very narrow, with a maximum at $\theta = \pi/2$.

Figures 5 and 6 show the horizontal and vertical far-field power patterns for the $N = 72$ array of Fig. 4 as calculated from (16)–(18). It is seen that Properties 5.2 and 5.3 hold.

The narrowness of the vertical beam can be estimated by neglecting variations of the field in (20) due to the slowly varying $G(\theta)$ and defining vertical directivity as the maximum of the array factor divided by its mean value, viz.,

$$D_V = \frac{|A^{(m)}(\pi/2,\phi)|}{\frac{1}{2}\int_0^\pi |A^{(m)}(\theta,\phi)| \sin\theta \, d\theta}. \tag{24}$$

Subject to the approximation (22), the integral can be carried out analytically and the resulting $D_V$ is independent of $\phi$ when $m \ll N/2$. Thus,

$$D_V = \frac{2J_m[N(d/\lambda)]}{\pi J_{(m-1)/2}[\frac{1}{2}N(d/\lambda)]J_{(m+1)/2}[\frac{1}{2}N(d/\lambda)]}; \qquad m \ll N/2. \quad (25)$$

With the asymptotic expression for the Bessel functions and after some manipulation,

$$D_V \sim (2N/\pi)^{1/2}[(m/N)^2 - (d/\lambda)^2]^{1/4}. \quad (26)$$

Hence,

Property 5.4: For a specific resonance $m/N$, making $N$ larger will result in a narrower vertical field pattern, and in more spikes in the azimuth.

Property 5.5: For fixed $N$ and for a specific phase-sequence resonance $m$, making the dipoles thicker or longer will result in a smaller resonant spacing $\delta_{m/N}$, a much narrower resonance, and a slightly more directive vertical field pattern.

The directivity may therefore be made arbitrarily large by making $N$ large (although the increase is slow, roughly as the square root of $N$). The field strength at any point in space increases very rapidly. The input impedance may be a pure resistance. However, the physical dimensions of the array increase (linearly with $N$) and the bandwidth decreases very rapidly.

The array factor's smallness has an interesting consequence. For resonant *noncircular* arrays, an array factor $A(\theta, \phi)$ may be defined as in (19). $A(\theta, \phi)$ will be a sum of $N$ terms of order 1, each term depending on the location of element $l$ and its relative current (admittance). If a sufficiently large noncircular array with one element driven is thought of as a perturbation of some corresponding circular array, it is logical to assume that the current distribution around the array will not be significantly affected and will again be of the standing-wave type. Hence, each term in the sum for $A(\theta, \phi)$ will be close to each

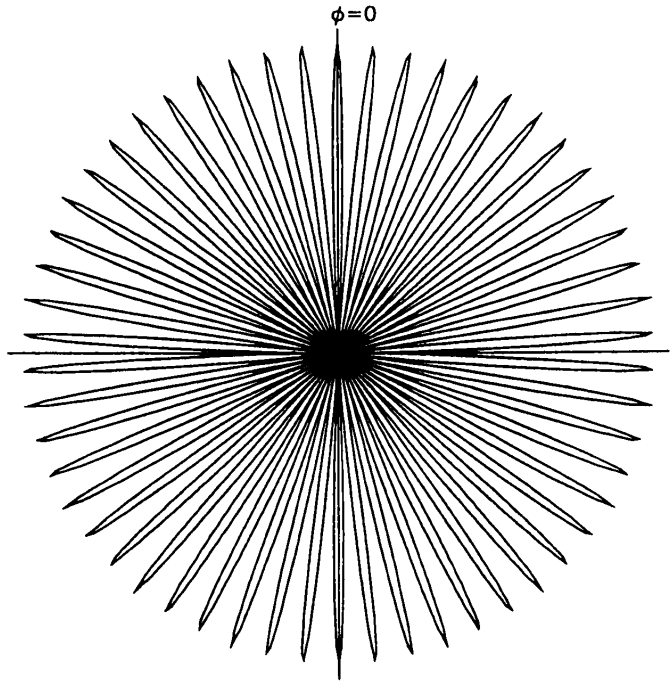


**Figure 5. Normalized far-field power pattern $|E(\pi/2, \phi)|^2$ at $\theta = \pi/2$ plane of dipoles' centers for $m = 27$ phase-sequence resonance; $N = 72$, $h/\lambda = 0.2$, $a/\lambda = 0.05$, and $d/\lambda = 0.22688$.**

term in the sum for the circular array. However, any very small quantity that can be written as the sum of terms of order 1 is extremely sensitive to perturbations of these terms. Therefore, the array factor (field pattern) for the noncircular array will not be close to that of the circular array. Thus, a wide variety of field patterns may be obtained by resonant noncircular arrays, perhaps even a superdirective pattern as proposed in [1].

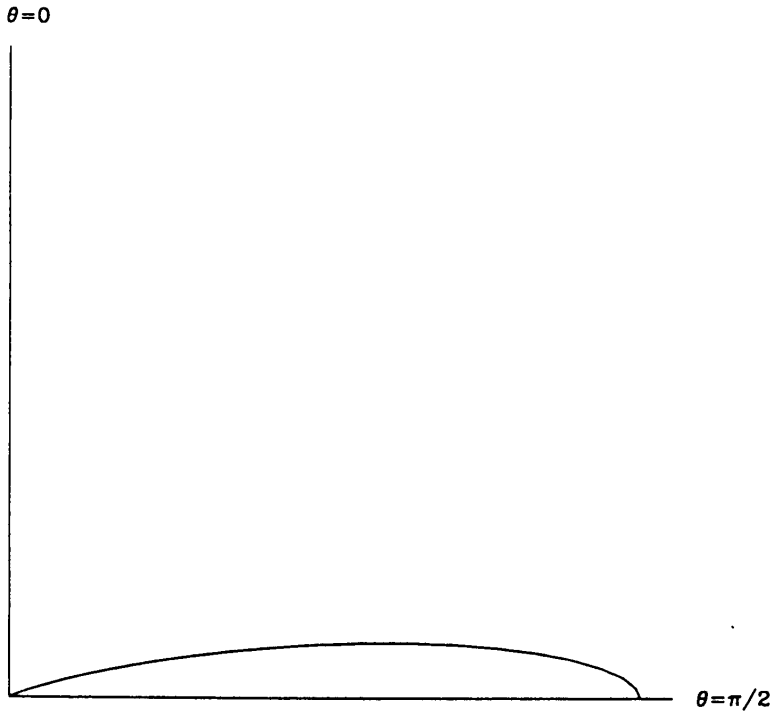


**Figure 6. Normalized far-field power pattern $|E(\theta,0)|^2$ at $\phi = 0$ for $m = 27$ phase-sequence resonance; $N = 72$, $h/\lambda = 0.2$, $a/\lambda = 0.05$, and $d/\lambda = 0.22688$.**

## 6. Refinements for Numerical Calculations

Two further improvements to the two-term theory are now presented. These do not change the properties given before but are useful for numerical calculations requiring high precision. These improvements apply specifically to thin-walled dipoles.

Whereas the real part of the self-term of the kernel $K_{1R}(z)$ given in (*B7*) assumes interaction from axis to perimeter, the more compli-

cated form (see Appendix A)

$$K_{1R}(z) = \frac{1}{2\pi}\int_{-\pi}^{\pi} \frac{\cos\{k[z^2+4a^2\sin^2(\phi/2)]^{1/2}\}}{[z^2+4a^2\sin^2(\phi/2)]^{1/2}}\,d\phi \tag{27}$$

assumes that the interaction is from a point on the perimeter to another point on the perimeter. The use of (27) instead of (*B*7) provides higher accuracy. A detailed discussion of this kernel for the case of a single driven element is provided in [16].

The second improvement comes from the observation that the trigonometric functions $\sin k(h-|z|)$ and $\cos kz - \cos kh$ are not adequate to describe the charge build-up near the ends of the element. It is known that $I(z)$ behaves like $\sqrt{h-|z|}$ for $|z|$ close to $h$ for both the driven [17] and the parasitic elements. A simple improvement to the current that takes into account this behavior is achieved [10], [18], by modifying the shifted cosine to

$$f(z) = \begin{cases} \cos kz - \gamma_1, & |z| < z_0, \\ \gamma_2\sqrt{kh - k|z|}, & z_0 < |z| < h, \end{cases} \tag{28}$$

where the constants $\gamma_1$, $\gamma_2$, and $z_0$ are found by matching $f$, $f'$, and $f''$ at $z = z_0$. The resulting equations are

$$\tan kz_0 = 2(kh - kz_0), \tag{29}$$

$$\gamma_1 = \cos kz_0[1 - 4(kh - kz_0)^2]; \qquad \gamma_2 = 2\sqrt{kh - kz_0}\sin kz_0. \tag{30}$$

Formula (29) is a transcendental equation which has exactly one solution for $kz_0$ when $kh < \pi/2$. The two-term solution then becomes (1)–(3) and (*B*1)–(*B*12) with $\cos kz - \cos kh$ in (1) and (*B*4)–(*B*6) replaced by $f(z)$ as given by (28)–(30).

| $m$ | $f_m^T$ (GHz) | $f_m^E$ (GHz) | Percentage Error |
|---|---|---|---|
| 29 | 2.4260 | 2.4311 | 0.214 |
| 30 | 2.4623 | 2.4681 | 0.236 |
| 31 | 2.4950 | 2.5009 | 0.237 |
| 32 | 2.5241 | 2.5298 | 0.227 |
| 33 | 2.5497 | 2.5554 | 0.224 |
| 34 | 2.5722 | 2.5777 | 0.215 |
| 35 | 2.5919 | 2.5970 | 0.199 |
| 36 | 2.6090 | 2.6137 | 0.182 |
| 37 | 2.6238 | 2.6288 | 0.189 |
| 38 | 2.6365 | 2.6413 | 0.183 |
| 39 | 2.6473 | 2.6519 | 0.176 |
| 40 | 2.6562 | 2.6602 | 0.153 |
| 41 | 2.6634 | 2.6678 | 0.165 |
| 42 | 2.6689 | 2.6728 | 0.146 |
| 43 | 2.6728 | 2.6765 | 0.139 |
| 44–45 | 2.6752 | 2.6791 | 0.147 |

**Table 2. Resonant Frequencies $f_m$: Theoretical ($f_m^T$), Experimental ($f_m^E$) (from the Data of [9]), and Percentage Error;** $N = 90$, $h = 0.858$in., $2a = 1/4in.$, **and** $2R = 40in.$

With these refinements, very good agreement between theory and experiment has been obtained. Theoretically predicted ( $f_m^T$ ) and measured ( $f_m^E$ ) resonant frequencies are compared in Table 2. The experiment is described in [9, Ch. 8]. The general layout is that of Fig. 2; the monopoles are made from brass and the ground plane is made from aluminum. The parameters of the experiment are $N = 90$, $h = 0.858$ in., $2a = 1/4$ in., and $2R = d/\sin(\pi/N) = 40$ in. Each $f_m^T$ is obtained as the root of $D_R^{(m)}$ as described in Section 3. Each $f_m^E$ corresponds to a maximum in the measured $G_{1,1}$. As explained in detail in [9], the last resonant frequencies ( $m = 44$–$45$) coincide. It is seen from Table 2 that the agreement is in all cases excellent, of the order of a fraction of a percent.

## 7. Conclusion

By analyzing and simplifying the two-term solution for the current distributions on a circular array of lossless dipoles, the properties of a large resonant circular array with one element driven have been derived. A variety of different resonances may be excited by suitable combinations of the many parameters of the problem. Each resonance is associated with extremely large self- and mutual conductances characteristic of a particular standing-wave distribution of the currents in the elements around the array. The self-susceptance varies rapidly with frequency and vanishes when the self-conductance is nearly at its maximum. The associated characteristic far-field pattern consists of a large number of narrow pencil-like beams. The analysis contained here supplements earlier investigations and is essential for the study of more complicated types of closed-loop arrays with potentially important applications. It is now possible to choose the parameters so that the resonances are much narrower than those illustrated in [7]. For the specific parameters of [7], however, the improved theory of the present paper does not predict very narrow resonances.

## Appendix A: The Various Kernels

Four different kernels for the $m^{\text{th}}$ phase-sequence integral equation are mentioned in this paper. Their relationship and applicability are discussed here. Consider the coupled integral equations for the current distributions $I_l(z)$ in an array of identical, perfectly conducting, parallel, nonstaggered tubular dipoles of radius $a$ and half-length $h$ (the array may or may not be circular, and more than one element may be driven):

$$4\pi\mu_0^{-1}A_{zl}(z) \equiv \sum_n \int_{-h}^{h} I_n(z')K_{nl}(z-z')\,dz'$$

$$= -\frac{j4\pi}{\zeta_0}\left(C_l \cos kz + \frac{V_l}{2}\sin k|z|\right). \qquad (A1)$$

In ( A1 ), the constants $C_l$ are determined from the conditions $I_l(h) = 0$, $A_{zl}(z)$ is the $z$-directed vector potential on the surface of dipole $l$, and $V_l$ is the voltage driving element $l$, with $V_l = 0$ if the element

is parasitic. Each term in the sum on the left-hand side of the integral equation is the vector potential on element $l$ due to the current $I_n(z')$ on element $n$; the kernel $K_{nl}$ associated with each vector potential is a "self-interaction kernel" if $n = l$ so that $K_{nl}(z) = K_{ll}(z) = K_{11}(z)$ or a "mutual interaction kernel" if $n \neq l$. The various $m^{\text{th}}$ phase-sequence kernels result from the following four sets of kernels:

1) The original kernels of [4],

$$K_{ll}(z) = \frac{\exp[-jk(z^2 + a^2)^{1/2}]}{(z^2 + a^2)^{1/2}}, \tag{A2a}$$

$$K_{nl}(z) = \frac{\exp[-jk(z^2 + b_{nl}^2)^{1/2}]}{(z^2 + b_{nl}^2)^{1/2}}; \qquad n \neq l, \tag{A2b}$$

where $b_{nl}$ is the distance between the axis of dipole $l$ and the axis of dipole $n$.

2) The improved kernels of [8] and [10],

$$K_{ll}(z) = \frac{1}{2\pi} \int_{-\pi}^{\pi} \frac{\exp\{-jk[z^2 + 4a^2 \sin^2(\phi'/2)]^{1/2}\}}{[z^2 + 4a^2 \sin^2(\phi'/2)]^{1/2}} d\phi', \tag{A3a}$$

$$K_{nl}(z) = \frac{1}{4\pi^2} \int_{-\pi}^{\pi} \int_{-\pi}^{\pi} \frac{e^{-jkR_{nl}(z,\phi,\phi')}}{R_{nl}(z,\phi,\phi')} d\phi' \, d\phi; \qquad n \neq l, \tag{A3b}$$

where

$$R_{nl}(z,\phi,\phi') = [z^2 + (a\sin\phi - a\sin\phi')^2 + (a\cos\phi - a\cos\phi' - b_{nl})^2]^{1/2} \tag{A3c}$$

is the distance between a point on the surface of dipole $l$ and the surface of dipole $n$.

3) The modified kernels of this paper. The mutual interaction kernels $K_{nl}(z)$ are in (A2b) and the self-interaction kernel is

$$K_{ll}(z) = \frac{\cos[k(z^2 + a^2)^{1/2}]}{(z^2 + a^2)^{1/2}} - j\frac{\sin kz}{z}. \tag{A4}$$

4) The refined modified kernels of Section 6 of this paper. The mutual interaction kernels are again the same as in (A2b) and the

self-interaction kernel is

$$K_{ll}(z) = \frac{1}{2\pi}\int_{-\pi}^{\pi} \frac{\cos\{k[z^2+4a^2\sin^2(\phi'/2)]^{1/2}\}}{[z^2+4a^2\sin^2(\phi'/2)]^{1/2}}\,d\phi' - j\frac{\sin kz}{z}. \quad (A5)$$

The improved kernels ( $A3a, b$ ) are, by nature of their derivation, inherently more accurate than the rest. However, they are significantly more complicated so that adequate simpler alternatives are needed. Note that the imaginary parts of ( $A2b$ ), ( $A4$ ), and ( $A5$ ) are equal to the corresponding imaginary parts of ( $A3a, b$ ) with the radius $a$ set to zero so that statements concerning the imaginary parts of the improved kernels may be specialized to obtain corresponding statements for the imaginary parts of the modified or refined modified kernels. This is not true, however, for the real parts.

For arrays of a small number of elements $N$, where narrow resonances do not occur, the original kernels ( $A2a, b$ ) are adequate. In particular, a detailed discussion of the relationship between ( $A2a$ ) and ( $A3a$ ) in the case $N = 1$ (where the latter kernel is exact) is given in [16]. It is believed that the use of any of the sets of kernels in approximate solutions to the integral equations such as the two-term theory would not make a noticeable difference when $N$ is small. Significant differences exist when $N$ is large and narrow resonances occur. The case of a non-driven infinite linear array and that of a large circular array will be examined in turn.

*Case 1.* It is shown in [8] and [10] that a nondriven infinite linear array of equispaced elements (here, $b_{nl} = |n-l|d$ ) may possess resonances of zero width where the currents satisfy $I_l^{(\beta)}(z) = I_0^{(\beta)}(z)e^{j\beta l}$. Thus, the integral equation for $I_0^{(\beta)}(z)$ is

$$\int_{-h}^{h} I_0^{(\beta)}(z')K^{(\beta)}(z-z')\,dz' = -\frac{j4\pi}{\zeta_0}C_0\cos kz, \quad (A6)$$

where

$$K^{(\beta)}(z) = \sum_{l=-\infty}^{\infty} K_{0l}(z)e^{j\beta l} = K_{00}(z) + 2\sum_{l=1}^{\infty} K_{0l}(z)\cos\beta l. \quad (A7)$$

It is shown in [8] and [10] that $K^{(\beta)}(z)$ is real for all $z$ when $d/\lambda < \beta/2\pi < \frac{1}{2}$ and when the improved kernels ( $A3a, b$ ) are used. It follows

that this is also true when the modified and refined modified kernels are used. Hence, with these kernels, ( $A6$ ) is a real equation and this suggests the possibility of real solutions $I_0^{(\beta)}(z)$ with $I_0^{(\beta)}(h) = 0$ for proper choices of $d/\lambda$, $h/\lambda$, and $a/\lambda$. However, $K^{(\beta)}(z)$ is not real if the original kernels ( $A2a, b$ ) are used, so that ( $A2a, b$ ) are inadequate in this case.

*Case 2.* Next consider the integral equations for the currents $I_l^{(m)}(z)$ in the $m^{\text{th}}$ phase sequence for a large circular array. The driving voltages (and, therefore, the currents) satisfy $V_l^{(m)} = V_1^{(m)} \exp[j2\pi(l-1)m/N]$ and the integral equation for $I_1^{(m)}(z)$ is

$$\int_{-h}^{h} I_1^{(m)}(z') K^{(m)}(z - z')\, dz' = -\frac{j4\pi}{\zeta_0}\left(C_1^{(m)} \cos kz + \frac{V_1^{(m)}}{2} \sin k|z|\right), \tag{A8}$$

where

$$K^{(m)}(z) = \sum_{l=1}^{N} K_{1l}(z) e^{j2\pi(l-1)m/N} = K_{11}(z) + \sum_{l=2}^{N/2+1} \xi_l K_{1l}(z) \cos\left[\frac{2\pi(l-1)m}{N}\right], \tag{A9}$$

and $\xi_l$ is defined in ($B10$). Here, the distances $b_{nl}$ are $b_{nl} = b_{1,l-n+1} = d \sin(|l-n|\pi/N)/\sin(\pi/N)$. It is shown in [8] and [10] that $\mathrm{Im}\{K^{(m)}(z)\}$ is exponentially small in $N$ for all $z$ when $d/\lambda < m/N < \frac{1}{2}$ and when the improved kernels ( $A3a, b$ ) are used; an asymptotic formula for $\mathrm{Im}\{K^{(m)}(z)\}$ is derived. The asymptotic formula (6) for $\mathrm{Im}\{K^{(m)}(z)\}$ when the modified or refined modified kernels are used may then be obtained from the results of [8] and [10]; $\mathrm{Im}\{K^{(m)}(z)\}$ is exponentially small in this case as well—the only difference is a small overall multiplicative factor of $J_0^2(ka)$. If the original kernels ($A2a, b$) were used, $\mathrm{Im}\{K^{(m)}(z)\}$ would not be exponentially small and this property is crucial for an accurate description of the resonances.

The preceding analysis shows that $(A4)$ or $(A5)$ together with $(A2b)$ are simpler, adequate alternatives to $(A3a,b)$ and that $(A2a,b)$ are not adequate for the cases of an infinite linear array or a large circular array. It is believed that these statements are also valid for large noncircular arrays. Note that all discussions up to this point concern the imaginary parts of the kernels only; $(A4)$ differs from $(A5)$ only in the real part. It seems logical to retain the "exact" real part of the self-interaction kernel for calculations where high precision is needed especially since the resulting two-term theory formulas are not much more complicated numerically. In any case, the refined modified kernels $(A5)$ and $(A2b)$ (together with the square-root end correction of Section 6) are the ones that give the best agreement between two-term theory calculations and the two experiments that have been performed [9,13].

## Appendix B: The Parameters in (1) and (3)

The full formulas for the parameters $\Psi_{dR}$, $P_{1R}$, $D_{1R}$, $P_{\Sigma R}^{(m)}$, $D_{\Sigma R}^{(m)}$, $P_I^{(m)}$, and $D_I^{(m)}$ appearing in (1) and (3) are given here. They are:

$$P_{1R} = \int_{-h}^{h} \sin k(h-|z|) K_{1R}(h-z)\, dz, \tag{B1}$$

$$P_{\Sigma R}^{(m)} = -\frac{1}{1-\cos kh} \int_{-h}^{h} \sin k(h-|z|) \times [\cos kh\, K_{\Sigma R}^{(m)}(z) - K_{\Sigma R}^{(m)}(h-z)]\, dz, \tag{B2}$$

$$P_I^{(m)} = -\frac{1}{1-\cos kh} \int_{-h}^{h} \sin k(h-|z|) \times [\cos kh\, K_I^{(m)}(z) - K_I^{(m)}(h-z)]\, dz, \tag{B3}$$

$$D_{1R} = \frac{1}{1-\cos kh} \int_{-h}^{h} (\cos kz - \cos kh) \times [\cos kh\, K_{1R}(z) - K_{1R}(h-z)]\, dz, \tag{B4}$$

$$D_{\Sigma R}^{(m)} = \frac{1}{1-\cos kh} \int_{-h}^{h} (\cos kz - \cos kh) \times [\cos kh\, K_{\Sigma R}^{(m)}(z) - K_{\Sigma R}^{(m)}(h-z)]\, dz, \tag{B5}$$

$$D_I^{(m)} = \frac{1}{1-\cos kh}\int_{-h}^{h}(\cos kz - \cos kh) \times [\cos kh\, K_I^{(m)}(z) - K_I^{(m)}(h-z)]\, dz. \qquad (B6)$$

The various parts of the modified kernel (the use of which is justified in Appendix A and [9] and [10]) are

$$K_{1R}(z) = \frac{\cos kR_1(z)}{R_1(z)}, \qquad (B7)$$

$$K_{\Sigma R}^{(m)}(z) = \sum_{l=2}^{N/2+1} \xi_l \cos\left[\frac{2\pi(l-1)m}{N}\right] \frac{\cos kR_l(z)}{R_l(z)}, \qquad (B8)$$

$$K_I^{(m)}(z) = -\frac{\sin kz}{z} - \sum_{l=2}^{N/2+1} \xi_l \cos\left[\frac{2\pi(l-1)m}{N}\right] \frac{\sin kR_l(z)}{R_l(z)}, \qquad (B9)$$

where

$$\xi_l = \begin{cases} 1, & l = N/2+1, \\ 2, & \text{otherwise}, \end{cases} \qquad (B10)$$

and

$$R_l(z) = (z^2 + b_l^2)^{1/2}; \qquad b_l = \begin{cases} a, & l = 1, \\ \dfrac{d\sin[(l-1)\pi/N]}{\sin(\pi/N)}, & l \neq 1. \end{cases} \qquad (B11)$$

Note that the radius $a$ does not appear in $(B9)$. Finally, the equation for $\Psi_{dR}$ is

$$\Psi_{dR} = \int_{-h}^{h}(\cos kz - \cot kh \sin k|z|) \times [K_{1R}(z) - K_{1R}(h-z)]\, dz. \qquad (B12)$$

## Acknowledgments

This research was supported in part by the U.S. Air Force under Rome Laboratory Contract F19628-91-K-0020 with Harvard University. Additional support was provided by the Joint Services Electronics Program under Grant N00014-89-J-1023 with Harvard University and AFOSR support of Rome Laboratory.

## References

[1] King, R. W. P., "Supergain antennas and the Yagi and circular arrays," *IEEE Trans. Antennas Propagat.*, Vol. AP–37, 178–186, 1989.

[2] Wu, T. T., "Fermi pseudopotentials and resonances in arrays," 293–306 in *Resonances–Models and Phenomena: Proceedings, Bielefeld 1984,* S. Albeverio, L. S. Ferreira, and L. Streit, Eds., Springer-Verlag, Berlin, 1984.

[3] Grossmann, A., and T. T. Wu, "A class of potentials with extremely narrow resonances," *Chin. J. Phys.*, Vol. 25, 129, 1987.

[4] King, R. W. P., R. B. Mack, and S. S. Sandler, *Arrays of Cylindrical Dipoles,* Chap. IV, Cambridge University Press, New York, 1968.

[5] Mailloux, R. J., "Antenna and wave theories of infinite Yagi-Uda arrays," *IEEE Trans. Antennas Propagat.*, Vol. AP–13, 499–506, 1965.

[6] Shefer, J., "Periodic cylinder arrays as transmission lines," *IEEE Trans. Microwave Theory Tech.*, Vol. MTT–11, 55–61, 1963.

[7] Fikioris, G., R. W. P. King, and T. T. Wu, "The resonant circular array of electrically short elements," *J. Appl. Phys.*, Vol. 68, 431–439, 1990.

[8] Freeman, D. K., and T. T. Wu, "An improved kernel for arrays of cylindrical dipoles," presented at the 1991 IEEE/AP-S Symposium, London, Ontario, June 24–28, 1991.

[9] Fikioris, G., Ph.D. thesis, Harvard University, 1993.

[10] Freeman, D. K., Ph.D. thesis, Harvard University, 1992.

[11] Fikioris, G., R. W. P. King, and T. T. Wu, "Resonant antenna arrays with pancake-shaped field patterns," presented at the 1993 IEEE/URSI Radio Science Meeting, Ann Arbor, Michigan, June 28–July 2, 1993.

[12] King, R. W. P., "Electric fields and vector potentials of thin cylindrical antennas," *IEEE Trans. Antennas Propagat.*, Vol. AP-38, 1456–1461, 1990.

[13] Shen, H.-M., "Experimental study of the resonance of a circular array," *Proceedings of the SPIE,* Vol. 1407, 306–315, 1991.

[14] King, R. W. P., "The large circular array with one element driven," *IEEE Trans. Antennas Propagat.*, Vol. AP-38, 1462–1472, 1990.

[15] Tillman, Jr., J. D., *The Theory and Design of Circular Antenna Arrays,* Univ. Tennessee Experiment Station, 1966.

[16] Wu, T. T., "Introduction to linear antennas," Ch. 8 in *Antenna Theory, Part I,* R. E. Collin and F. J. Zucker, Eds., McGraw-Hill Book Co., New York, 1969.

[17] Shen, H.-M., and T. T. Wu, "The universal current distribution near the end of a tubular antenna," *J. Math. Phys.*, Vol. 30, 2721–2729, 1989.

[18] Freeman, D. K., and T. T. Wu, "Variational principle formulation of the two-term theory for arrays of cylindrical dipoles," *IEEE Antennas Propagat.*, submitted for publication.